

Ni-Zn-[Fe₄-S₄] and Ni-Ni-[Fe₄-S₄] clusters in closed and open α subunits of acetyl-CoA synthase/carbon monoxide dehydrogenase

Claudine Darnault^{1,2}, Anne Volbeda^{1,2}, Eun Jin Kim³, Pierre Legrand¹, Xavier Vernède¹, Paul A. Lindahl³ and Juan C. Fontecilla-Camps¹

Published online 10 March 2003; doi:10.1038/nsb912

The crystal structure of the tetrameric $\alpha_2\beta_2$ acetyl-coenzyme A synthase/carbon monoxide dehydrogenase from *Moorella thermoacetica* has been solved at 1.9 Å resolution. Surprisingly, the two α subunits display different (open and closed) conformations. Furthermore, X-ray data collected from crystals near the absorption edges of several metal ions indicate that the closed form contains one Zn and one Ni at its active site metal cluster (A-cluster) in the α subunit, whereas the open form has two Ni ions at the corresponding positions. Alternative metal contents at the active site have been observed in a recent structure of the same protein in which A-clusters contained one Cu and one Ni, and in reconstitution studies of a recombinant apo form of a related acetyl-CoA synthase. On the basis of our observations along with previously reported data, we postulate that only the A-clusters containing two Ni ions are catalytically active.

Acetyl-coenzyme A (CoA) synthase/carbon monoxide dehydrogenase (ACS/CODH) is a bifunctional enzyme that catalyzes the reversible reduction of CO₂ to CO (CODH activity):



In addition, ACS/CODH catalyzes the synthesis of acetyl-CoA from CO, CoA and a methyl group donated by the cobalt-containing corrinoid iron-sulfur protein (CoFeSP) (ACS activity). Such activities have been implicated in the 'Fe-S World' theory of the origin of life in which fixing CO₂ into activated acetyl groups on (Ni)Fe-S surfaces is thought to have produced autocatalytic metabolites¹. The ACS/CODH enzyme from the acetogenic bacterium *Moorella thermoacetica* (ACS/CODH_{Mt}) is a 310 kDa $\alpha_2\beta_2$ tetramer that plays a central role in synthesizing acetyl-CoA through the Wood/Ljungdahl pathway². The β subunits of ACS/CODH_{Mt} are homologous to homodimeric CODH enzymes found in carboxydophilic bacteria, including *Rhodospirillum rubrum* (Rr) and *Carboxythermus hydrogenoformans* (Ch); these homodimeric CODH enzymes catalyze reaction (1) but not the synthesis of acetyl-CoA from CO^{3,4}. Each β subunit contains an [Fe₄-S₄] B-cluster and a novel active site [Ni-Fe₄-S_{4-or-5}] C-cluster. A single [Fe₄-S₄] D-cluster bridges the two β subunits. Each α subunit of ACS/CODH_{Mt} contains a single metal center, the A-cluster, which is responsible for the ACS activity⁵. During catalysis, CO that is generated by reducing CO₂ at the C-cluster migrates through a tunnel and binds to the A-cluster⁶⁻⁸, which also gets methylated by CH₃-Co³⁺FeSP^{9,10}. Methyl migration/CO insertion forms a metal-bound acetyl group that is attacked by CoA to generate acetyl-CoA^{7,10-12}. A recently determined structure of ACS/CODH_{Mt} has suggested that the A-cluster consists of a Ni-Cu-[Fe₄-S₄] center⁸.

Here we report the crystal structure of CO-treated ACS/CODH_{Mt} solved at 1.9 Å resolution. Surprisingly, and contrary to the recently reported structure of the same enzyme⁸, the two α subunits display different conformations and have A-clusters with dissimilar coordination geometries and metal contents. On the basis of these observations, we discuss possible catalytic mechanisms for the synthesis of acetyl-CoA. In addition, we show that the hydrophobic tunnels connecting the C- and A-clusters extensively bind Xe, a heavy gas that mimics the affinity of CO for such tunnels.

Structure determination

The structure of ACS/CODH_{Mt} was initially solved by a combination of molecular replacement (MR) using the CODH_{Ch} model and a MAD experiment performed at the Fe edge using native crystals. The model was progressively completed starting with the β subunits and followed by the N-terminal domain of the α subunits. Subsequently, the central and C-terminal domains of the α subunits could be built into an electron density map calculated with a combination of partially refined model and experimental phases. The current 1.9 Å resolution CO-treated ACS/CODH_{Mt} model, which includes all the protein atoms and >1,200 solvent molecules, has excellent refinement statistics and stereochemistry (see Methods).

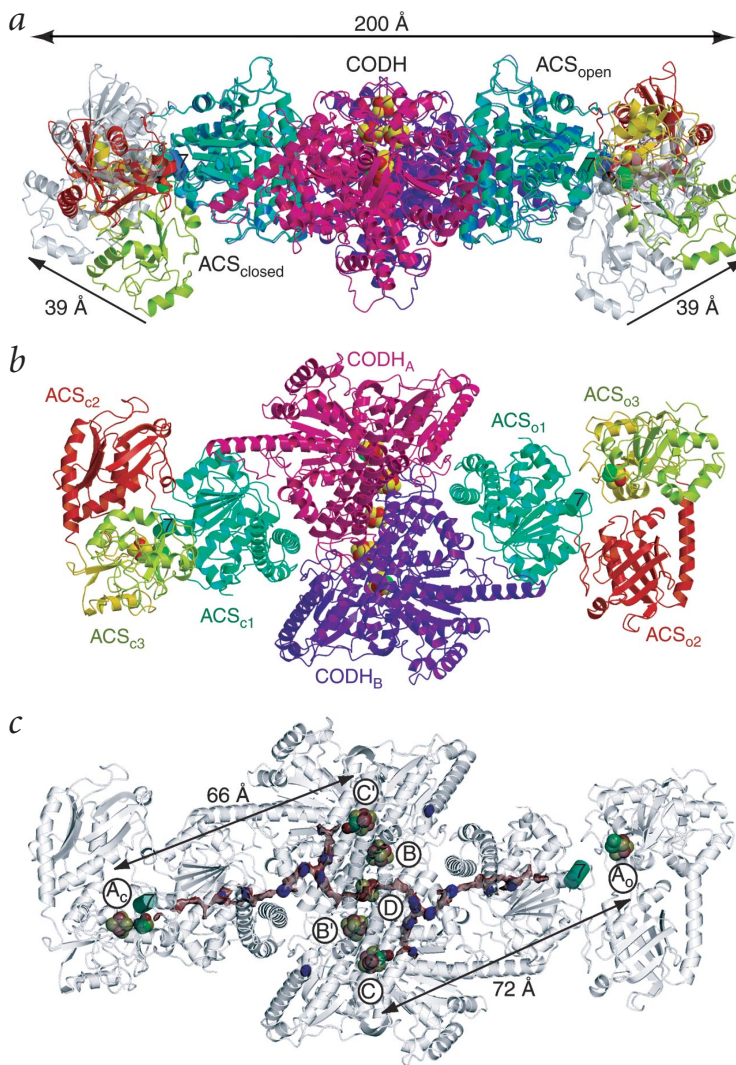
Description of the ACS/CODH_{Mt} atomic model

The overall quaternary structure and organization of subunits is similar to that observed by Doukov *et al.*⁸: an $\alpha_2\beta_2$ tetrameric enzyme with dimensions of ~200 × 75 × 105 Å (Fig. 1a,b). The two β subunits contact each other extensively, yielding a structure similar to the reported structures of CODH_{Ch} and CODH_{Rr}^{3,4}. The subunits are attached to opposite faces of the β_2

¹Laboratoire de Cristallographie et Cristallogénèse des Protéines, Institut de Biologie Structurale 'Jean-Pierre Ebel', CEA, UJF, CNRS, 41, rue Jules Horowitz, 38027, Grenoble Cedex 1, France. ²These two authors contributed equally to this work. ³Department of Chemistry, Texas A&M University, College Station, Texas 77843, USA.

Correspondence should be addressed to J.C.F.-C. e-mail: juan@lccp.ibs.fr

Fig. 1 Fold of the ACS/CODH $\alpha_2\beta_2\alpha_2$ tetramer in the monoclinic (C2) crystal form. Ribbons and arrows depict α -helices and β -strands, respectively. Metal sites are shown as spheres, using the following colors: S, yellow; Fe, red; Ni, green; and Zn, black. **a**, View with the molecular two-fold symmetry axis in the vertical direction. The two β subunits are shown in pink and violet, and the α subunit is shown in blue-green (domain 1, residues 1–312), red (domain 2, 313–478), yellow (domain 3a, 479–585) and light green (domain 3b, 586–729). In addition, a superposition is shown in blue (domain 1) and light gray (domains 2 and 3) of the α_c and α_o subunits after application of the molecular two-fold symmetry operation relating the β subunits. **b**, Perpendicular view relative to (a). **c**, Hydrophobic channels (pink) and electron density of Xenon sites (blue, contoured at the 4 σ level) as obtained in a $m(F_{Xe} - F_{native})$ difference Fourier using refined model phases. Channels were calculated from the refined model with CAUVEN^{48,49} using a probe radius of 0.8 Å. The mobile helix of the N-terminal domain of the α subunits is highlighted as a cylinder. In α_o , this helix occupies a position that blocks the channel entrance at the A_o site. This figure, along with Figs. 2–4, was made with MolScript⁵⁰, Raster3D⁵¹ and CONSCRIPT⁵².



unit and do not contact each other. The α subunits consist of three structural domains, designated as residues 1–312, 313–478 and 479–729. Only the N-terminal domain interacts with the β subunit. In contrast to the structure reported by Doukov *et al.*⁸, the α subunits in our structure have different conformations; packing analysis shows that they are not interchangeable in the crystal. As a consequence, the β subunits and most of the N-terminal domains of the α subunits satisfy the local two-fold symmetry axis of the $\alpha_2\beta_2$ dimer, whereas the remainder of each α subunit does not (Fig. 1a,b). The two α subunits differ by a rotation of $\sim 50^\circ$ about a region found at the interface of the N-terminal and central domains. The central and C-terminal domains move as rigid bodies and are not significantly modified by the rotation. The α subunit N-terminal domain is also largely unaffected by the rotation, except for a helical segment discussed below.

The conformation of the α subunits in the ‘closed’ conformation (α_c), seems to be similar to that reported by Doukov *et al.*⁸, whereas the other in the ‘open’ (α_o) conformation, has a larger exposed surface and allows greater solvent accessibility to the A-cluster. We will also designate the corresponding clusters as A_o and A_c and the tetramer as $\alpha_o\beta_2\alpha_c$.

Hydrophobic tunnel network and Xe sites

The enzyme contains an extensive cavity network (Fig. 1c). A central S-shaped region runs from one C-cluster to the other, opening near to the Ni ions of these clusters. At the quarter positions of this S are long branches leading to each A-cluster. One branch opens near the A_c -cluster, but the other is blocked ~ 20 Å from the A_o -cluster by the movement of the α subunit N-terminal domain helix comprising residues 143–148. The entire network follows the symmetry of the $\alpha_o\beta_2\alpha_c$ tetramer and runs approximately along a single plane through the molecule, as observed in NiFe hydrogenases¹³. Data from a crystal exposed to ten bar of Xe pressure before flash-cooling in a glove box show that there are two sets of eight Xe sites related by the local two-fold symmetry axis, seven of which are located in the tunnels connecting A- and C-clusters. When these tunnels are compared with those of the monofunctional CODH_{Ch}³, it is clear that the two enzymes have

evolved to guide intramolecular CO diffusion in different directions (data not shown).

The A-clusters of the α subunits

The most surprising observation concerning the two conformations displayed by the α subunit in our crystals is that the corresponding A-clusters are fundamentally different (Fig. 2). We have performed a series of anomalous scattering experiments to determine the nature of the metal centers present in the A-clusters by collecting X-ray data at the high energy side of the absorption edge for possible candidates, such as Fe, Co, Ni, Cu and Zn (Table 1). Double difference anomalous electron density maps indicate that the A_c -cluster is composed of a standard [Fe₄-S₄] cubane bridged by a cysteine thiolate to a proximal (relative to the cubane) Zn ion that, in turn, connects to a distal Ni ion (Ni_d) through two additional bridging cysteines (Fig. 2a). The distorted tetrahedral coordination of the Zn ion is completed by a tightly bound and apparently heterodiatomous exogenous ligand of unknown identity (Fig. 2c) that sits at the entrance of the hydrophobic tunnel mentioned above. The Ni_d ion has square planar coordination including, in addition to the two thiolates of Cys595 and Cys597, the two main chain N atoms from Gly596 and Cys597.

In the A_o -cluster, both the [Fe₄-S₄] cubane and the Ni_d ion with its S₂N₂ square planar coordination are preserved, whereas

Table 1 Metal assignments from anomalous diffraction experiments.

$\Delta_{\text{anom},\lambda}$ maps ¹	f''_{Zn} ²	f''_{Cu}	f''_{Ni}	f''_{Fe}	$\langle \rho / \sigma \rangle_{\text{Fe}}$ ³	$\langle \rho / \sigma \rangle_{\text{Ni}}$	$\rho / \sigma_{\text{Mpc}}$ ⁴	$\rho / \sigma_{\text{Mdc}}$ ⁴	$\rho / \sigma_{\text{Mpo}}$ ⁴	$\rho / \sigma_{\text{Mdo}}$ ⁴
$\Delta_{0.934}$ (CO _a data)	2.29	2.03	1.79	1.38	11.8	3.3	23.7	22.3	11.5	11.6
$\Delta_{1.282}$ (Zn edge)	3.88	3.41	3.04	2.36	11.2	9.0	22.1	19.8	10.2	13.0
$\Delta_{1.376}$ (Cu edge)	0.55	3.87	3.42	3.04	10.5	9.4	4.5	17.9	9.4	12.6
$\Delta_{1.482}$ (Ni edge)	0.63	0.55	3.89	3.40	12.3	10.5	3.7	25.7	8.3	18.2
$\Delta_{1.602}$ (Co edge)	0.73	0.63	0.55	3.91	11.0	0.9	1.8	3.3	-0.5	0.9

¹ λ is the X-ray wavelength (Å).

² f'' is the imaginary component of the anomalous scattering factor.

³ ρ is the electron density, and σ is the r.m.s. value of the map.

⁴M_p and M_d correspond to the proximal (with respect to the [Fe₄-S₄] cluster) and distal metal center, respectively, with c and o designating closed and open forms of the α subunit.

the proximal site is occupied by a square planar Ni ion (Ni_p) coordinated by the three μ^2 -bridging cysteine thiolates and an unidentified exogenous ligand (Fig. 2*b,d*). The superposition of the A_c- and A_o-clusters shows that the thiolate ligands, Ni_d and the Cys595–Cys597 region occupy positions that differ by a maximum of ~0.3 Å in the two clusters. In contrast, the position of the metal ion bound at the proximal site differs by ~1.3 Å (Fig. 3), accounting for the transition between the distorted tetrahedral and square planar coordinations. In the A_o-cluster, a significant residual peak in the $F_o - F_c$ electron density map suggests a partially occupied second position for the proximal metal ion that coincides with that of the Zn ion of the superimposed A_c-cluster (Fig. 3). Although we have not been able to use anomalous dispersion effects to identify the atom generating this peak, both Zn and Ni are plausible candidates, with occupancies of ~0.3 according to the crystallographic refinement.

Because Cu¹⁺ has been reported to be an essential component of the A-cluster⁸, double difference anomalous maps were calcu-

lated from data collected at both low ($\lambda = 1.482$ Å) and high ($\lambda = 1.376$ Å) energy sides of the Cu absorption edge. However, no significant positive peak was observed in the [$\Delta_{\text{anom}1.376} - \Delta_{\text{anom}1.482}$] double difference Fourier map, thereby ruling out the presence of any significant amounts of Cu in our A-clusters.

The source of the two different types of A-clusters in our crystals is not known. One possible explanation is that before crystallization, the A-clusters of the two α subunits of the heterodimer contained all combinations of metals: (Zn, Zn), (Zn, Ni) and (Ni, Ni). Either the crystal packing favored one of these forms directly (by selecting (Zn, Ni) with closed and open conformations, respectively) or, alternatively, the packing of the enzyme with one closed and one open form induced a rearrangement of metal ions at the metal centers in the crystal resulting in the observed distribution. A second alternative is that all the molecules in the crystallizing solution had the (Zn, Ni) configuration observed in our crystals, which may correspond to the natural active enzyme. The presence of an

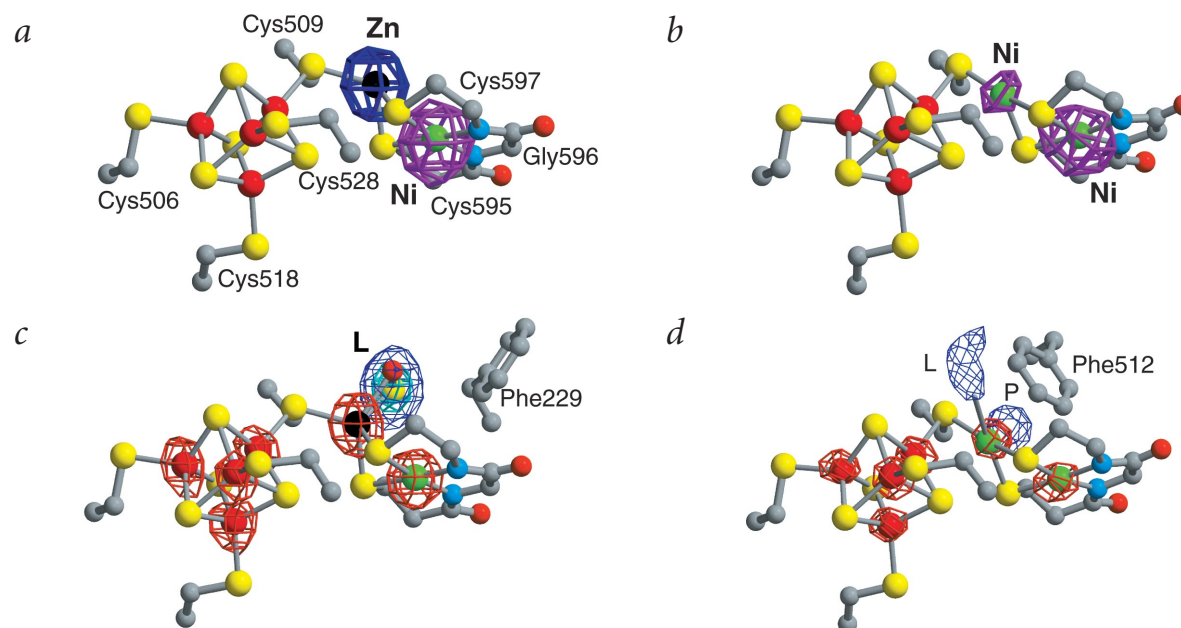


Fig. 2 Structure of the A-clusters in the α_c and α_o subunits depicted as ball-and-stick models. Atoms are colored as follows: Fe, red; Ni, green; Zn, black; S, yellow; O, orange; N, blue; and C, gray. **a**, The A_c-cluster. Double difference [$\Delta_{\text{anom}1.282} - \Delta_{\text{anom}1.376}$] (blue) and [$\Delta_{\text{anom}1.482} - \Delta_{\text{anom}1.602}$] (purple) anomalous electron density maps were solved at 2.7 Å resolution using data and 90°-shifted refined model phases from crystal CO_b (Table 2). These maps, contoured at the 4 σ level, show the presence of Zn and Ni at the proximal and distal sites, respectively (see also Table 1). **b**, The A_o cluster. The [$\Delta_{\text{anom}1.482} - \Delta_{\text{anom}1.602}$] anomalous electron density map shows the presence of two Ni ions. **c**, Same as (a), except that the maps shown are the $\Delta_{\text{anom}0.934}$ difference map (red) calculated using refined 1.9 Å resolution model phases and the corresponding $mF_o - F_c$ map⁴⁶ that was contoured at the 4 σ (blue) and 10 σ (cyan) levels. The electron density shows the presence of an unidentified heteroatomic exogenous ligand (L) bound to Zn and modeled as SO. The Zn ion has distorted tetrahedral coordination. **d**, Same model as (b) depicting maps calculated in (c). The proximal Ni has square planar coordination and binds three cysteine thiolates and an exogenous ligand (L) of unknown nature but probably different from the one in (c). A residual electron density peak (P) that occupies a position equivalent to that of the Zn ion in (a) and (c) is also shown.

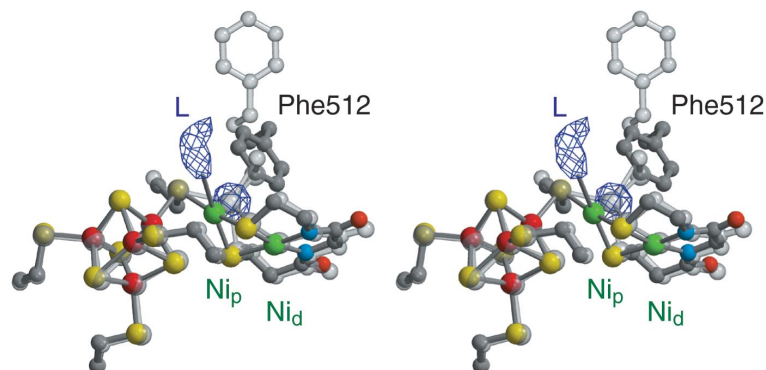


Fig. 3 Stereo view of a superposition of the A_0 - and A -clusters. The coordination of Ni_p in the A_0 cluster (atoms color-coded as in Fig. 2) indicates a square planar arrangement with three cysteine thiolates and one unidentified exogenous ligand (L). In the A -cluster (gray), the coordination of the proximal Zn ion is distorted tetrahedral (see also Fig. 5b). A 7σ electron density peak is found in a $mF_o - F_c$ map that is 1.3 \AA removed from Ni_p and that occupies, as shown, a position equivalent to the Zn in the A -cluster.

alternative position in the proximal metal of the A_0 -cluster (Fig. 3) that could be occupied by either Zn or Ni complicates the interpretation.

Metal clusters in the β subunit

Distances between the B-, C- and D-clusters of the β subunits of ACS/CODH_{Mt} are similar to those already reported for other CODHs^{3,4}. The C-cluster consists of a Ni-Fe₄-S₄ cage that can be viewed as a [Ni-Fe] subsite linked by three μ^3 -bridging sulfide ions emanating from one face of an [Fe₃-S₄] subsite. The Ni is four-coordinate with distorted tetrahedral geometry, including three endogenous ligands (the thiolate of Cys550 and two of the three μ^3 -bridging sulfide ions) and one unidentified exogenous axial ligand best modeled as CO with 0.5 occupancy (Fig. 4a). The unique Fe is coordinated by His283, Cys317 and the remaining μ^3 -bridging sulfide ion. Overall, our C-cluster is closer to the one reported by Drennan *et al.*⁴ in that it lacks the μ^2 -sulfide ion that bridges the Ni and unique Fe in CODH_{Ch}. There are several residual electron density peaks in our final $F_o - F_c$ difference Fourier electron density map indicating alternative conformations for some of the C-cluster atoms. These are generally difficult to model except for the peak between one sulfide of the [Fe₃-S₄] subsite and Cys316, suggesting a partially occupied persulfide and another peak that corresponds to an alternative position of the unique Fe (Fig. 4b). In our crystals, the C-cluster Ni ion is either disordered or only partially occupied because an electron density map containing no negative peak at the Ni site is obtained only when Ni occupancy is set to 0.5. Even the [Fe₃-S₄] subsite and the unique Fe are best modeled with 0.75 occupancies. A similar situation was observed in the CODH_{Ch} structure with a reported 0.80 occupancy for the C-cluster (PDB entry 1JYY). A detailed discussion of the structure/function relationships of the C-cluster will be reported elsewhere.

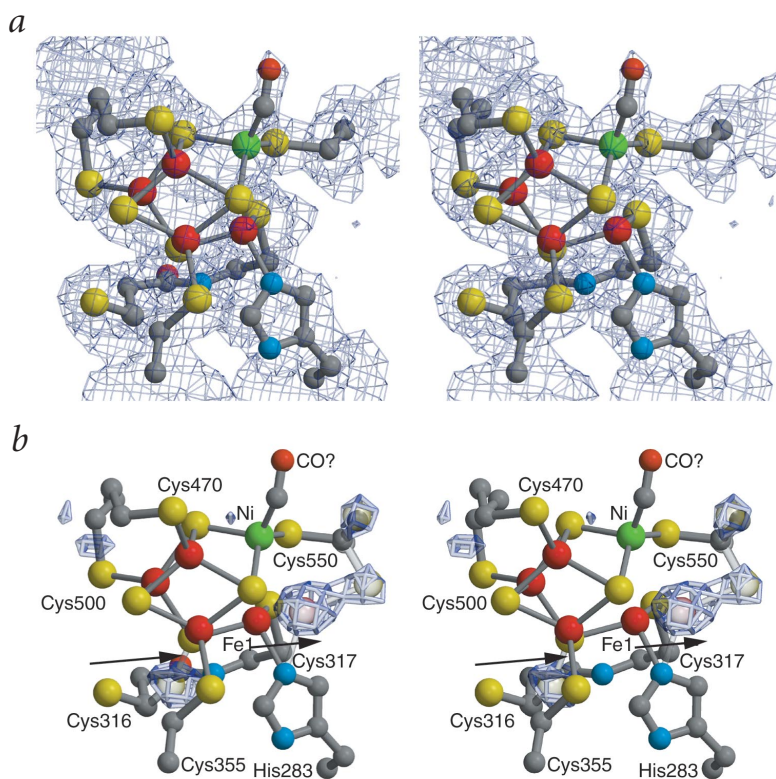


Fig. 4 Stereo views of the structure of the C-cluster in the β subunit. **a**, Electron density, contoured at the 1σ level, corresponding to a $2mF_o - DF_c$ difference electron density map⁴² using 1.9 \AA resolution refined model phases of CO-treated crystal CO_a. **b**, Residual $mF_o - F_c$ electron density peaks, contoured at the 5.5σ level, corresponding to (i) a putative persulfide formed between a labile S atom and Cys316, (ii) an alternative position for the unique Fe, as indicated by arrows and (iii) alternative conformations of Cys550. Atoms at alternative positions are shown as translucent spheres. Atoms are colored as in Fig. 2.

Properties of A-clusters

Known properties of the A-cluster are instrumental in relating the structure to a plausible mechanism of catalysis. A-clusters can be stabilized in at least two redox states, called A_{ox} ($S = 0$) and A_{red-CO} ($S = 1/2$)¹⁴. The reduction of A_{ox} to A_{red-CO} is mediated by one electron that is most likely generated by the oxidation of CO at the C-cluster. The [Fe₄-S₄]²⁺ cube is also reduced by one electron but the rate is too slow for reduction to occur with each catalytic cycle¹⁵. Both ACS/CODH_{Mt} and the isolated α subunit can accept a methyl group from $CH_3\text{-Co}^{3+}\text{FeSP}$ to form a stable methylated intermediate, but only after a reduction occurs at or near the A-cluster^{10,15,16}. No EPR signal associated with this process has been observed¹⁰, suggesting a two-electron oxidation-reduction with $S = 0$ or integer in both states. The A_{red-CO} state shows the well-studied Ni-Fe-C EPR signal, which broadens by hyperfine interactions in samples of *M. thermoacetica* grown on ⁶¹Ni ($I = 3/2$) or ⁵⁷Fe ($I = 1/2$) or in samples exposed to ¹³CO (refs. 17,18). Mössbauer and UV-visible studies indicate that the cube is in the 2+ state, suggesting that Ni is 1+ (refs. 19,20). The EPR signal along with acetyl-CoA synthase activity are abolished after oxidized ACS/CODH_{Mt} is treated with 1,10-phenanthroline (phen) because this chelator removes Ni from the A-cluster^{14,21,22}. The reaction is reversible, in that incubating phen-treated ACS/CODH_{Mt} with NiCl₂ under reduc-

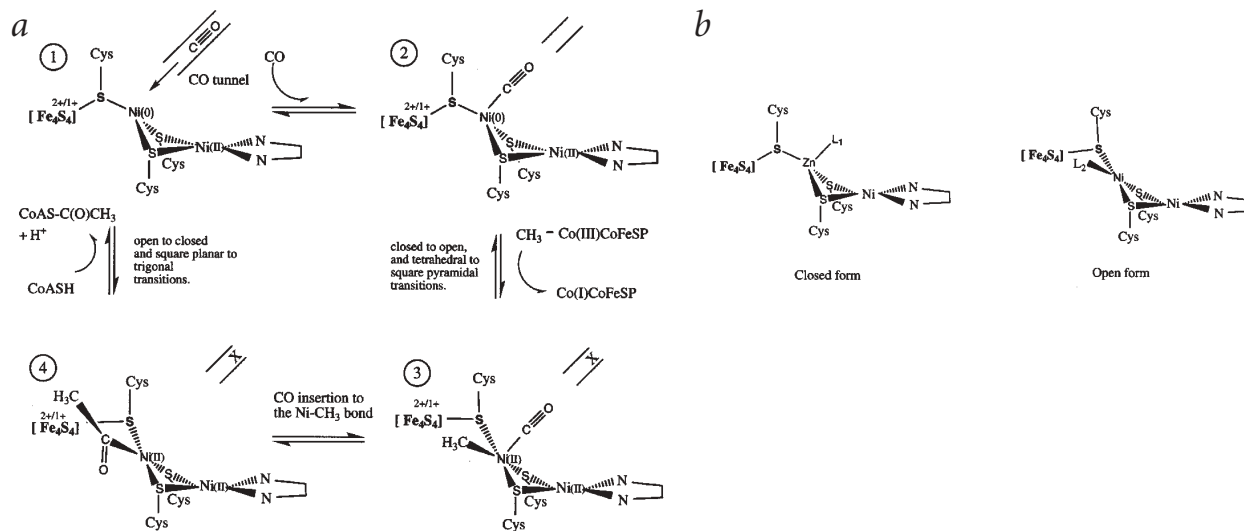


Fig. 5 Proposed catalytic mechanism and schematic representation of the A-clusters. **a**, A simple depiction of a plausible catalytic mechanism based on the closed and open structures of ACS and on available data concerning the possible redox properties of the metal centers of the A-cluster. In reaction **1** to **2**, CO produced at the C-cluster of the β subunit comes out of the tunnel and binds to trigonal pyramidal $Ni_p(0)$. In steps **2** to **3**, ACS goes from the closed to the open form (closing the CO tunnel), and Ni_p goes from tetrahedral to distorted square pyramidal coordination, generating an exposed equatorial site that binds CH_3^+ from CoFeSP while Ni_p goes from $Ni(0)$ to $Ni(II)$ to provide the required two electrons. Ni oxidation and the tetrahedral-to- CH_3 -bound-square planar coordination change are probably concerted as $Ni(0)$ would prefer the former and $Ni(II)$ the latter. In the reaction of **3** to **4**, the axially bound CO inserts into the Ni- CH_3 bond generating an acetyl group exposed to the solvent medium. From step **4** to **1**, deprotonated CoA-S⁻ attacks the carbonyl carbon and forms acetyl-CoA, Ni_p is reduced to $Ni(0)$, the Ni_p coordination reverts to trigonal pyramidal and ACS adopts the closed conformation opening the CO tunnel as a new cycle starts. The $[Fe_4-S_4]$ cluster is depicted as $2+/1+$ in all the steps of the reaction to indicate that, although we do not know its valence during catalysis, methylation can take place whether the cluster is reduced or not¹⁵. The mechanism assumes that the α subunit stays open between methylation and CoA acetylation. There are at least two ways to picture CoA binding: either it binds to open α subunit productive site upon CoFeSP dissociation or, as suggested by the structure, the α subunit is forced to stay in an open configuration after methylation because of steric clash between the side chain of Ile146 and the methyl group bound to Ni_p that would result for the methylated A-cluster in the closed conformation. It is also possible to postulate methylation before CO binding, followed by partial closing of the α subunit and carbonylation of the A-cluster; however, the structure itself does not provide direct evidence concerning the order of events during catalysis. The reported A(ox) and A(red)-CO states¹⁴ are not catalytic intermediates in the model shown, and are not illustrated. **b**, Schematic depiction of the A-clusters in the closed and open conformations. L_1 and L_2 are unidentified exogenous ligands. From their corresponding electron densities, they seem to be different. The two A-cluster forms are the basis for the mechanism proposed in (a). If the reduced Ni_p site is tetrahedral (as in the closed Zn-containing form) and oxidized Ni_p is square planar (as in the open form), it is easy to rationalize why only the latter is extractable by phen¹⁴ based on their relative exposures to solvent.

ing conditions quantitatively restores Ni-Fe-C signal intensity and catalytic activity. Ni quantitation and studies with radioactive ⁶³Ni demonstrate that only ~0.2 Ni per $\alpha\beta$ subunit are removed/reinserted²². This indicates that the purified ACS/CODH_{Mt} contains two Ni populations: ~30% Ni is labile, catalytically active and displays the Ni-Fe-C signal, whereas the remaining nonlabile 70% Ni is catalytically and spectroscopically inactive.

The α_o subunit contains a pocket that may be of the appropriate size for $CH_3-Co^{3+}FeSP$ binding, a requirement for methylation. The A_o -cluster proximal Ni is located at the base of this pocket, exposed on the molecular surface and coordinated by only three protein thiolates. These features are consistent with Ni_p being extractable by phen after enzyme oxidation and, thus, being the labile Ni associated with the enzymatic activity. The distal Ni, which is less exposed to the solvent medium, has a square-planar geometry with an N_2S_2 donor set and consequently may be the nonlabile Ni. Indeed, XAS studies of phen-treated enzyme have suggested a square-planar N_2S_2 ligand set for the nonlabile Ni²⁰. Further evidence for the association of the partially occupied labile Ni with CO-binding and enzymatic activity is given by the Ni-Fe-C EPR signal mentioned above that in the purified enzyme has an intensity that corresponds to ~0.3 spin per $\alpha\beta$ subunit rather than the expected 1 spin per $\alpha\beta$ ^{5,23} and by quantitation of the amounts of CH_3 and CoA that bind to the enzyme (0.5 and 0.2 per $\alpha\beta$, respectively)^{10,22,24}.

Catalytic role of the A-cluster metal ions

Any proposed mechanism for acetyl-CoA synthesis by ACS is expected to provide a source for the two e^- (the previously postulated D-site¹⁰) that are required to form the metal-methyl bond at the A-cluster (Fig. 5a). Because of the absence of any potential electron donors near the A-cluster, the reducing functionality is likely related to redox changes at the cluster itself. As mentioned above¹⁵, the $[Fe_4-S_4]^{2+}$ cube is an unlikely candidate because it reduces at a rate 200-fold slower than methyl transfer. The presence of a Ni-Ni unit bridged by thiolates raises the possibility of a reduced spin-coupled $Ni_p^{1+}-Ni_d^{1+}$ arrangement that could oxidize to $Ni_p^{2+}-Ni_d^{2+}$ upon methylation. However, based on its N_2S_2 coordination sphere (with deprotonated N ligands from the protein main chain), Ni_d will not reduce to 1+ and, consequently, it likely remains as a diamagnetic square planar Ni^{2+} throughout catalysis. For Ni_p , we have direct evidence for coordination changes at the proximal site, as indicated by our open and closed α subunit conformations. If these are functionally relevant, they may be related to the redox state of Ni_p . Having ruled out $[Fe_4-S_4]$ and Ni_d as participating in the intramolecular redox events occurring with each catalytic cycle, we now propose that the Ni_p exists in at least two stable redox states: in the absence of reductants, it is in the 2+ state, but in the presence of CO *in vitro*, Ni_p^{2+} can be reduced by one electron and bind CO, yielding $Ni^{1+}-CO$ and the A_{red}-CO state. Both *in vivo* and *in vitro* in the presence of $CH_3-Co^{3+}FeSP$, CoA

Table 2 Data and refinement statistics¹

Data collection									
Crystal	Native	MAD-Fe ²		Xe	CO _a		CO _b ³		
Unit cell dimensions									
<i>a</i> (Å)	246.0	246.6	244.9	244.6			244.7		
<i>b</i> (Å)	81.7	81.9	81.5	81.9			81.2		
<i>c</i> (Å)	168.1	168.3	165.7	167.2			166.8		
β (°)	95.7	95.8	95.2	96.2			95.7		
ESRF beam line	BM30A	BM30A		BM30A	ID14EH1		ID29		
Wavelength (Å)	0.9801	1.7410	1.7430	1.7430	0.9340	1.2815	1.3762	1.4824	1.6020
Resolution (Å)	20–2.2	15–2.95	15–2.95	20–3.5	30–1.9	30–2.7	30–2.7	30–2.7	30–2.7
Unique reflections	150,825	129,302	126,252	72,344	239,946	171,815	170,327	168,095	166,445
Completeness (%) ⁴	90.6 (61.5)	93.9 (53.2)	91.8 (42.8)	89.0 (85.1)	94.4 (67.9)	97.9 (96.2)	97.1 (89.9)	95.8 (85.5)	94.9 (79.4)
Multiplicity	3.1	1.8	1.6	1.5	1.8	1.9	1.9	1.9	1.9
R _{sym} ⁴	4.7 (18.3)	4.3 (23.5)	4.6 (27.7)	10.0 (23.4)	5.3 (23.8)	4.5 (12.0)	5.0 (15.0)	4.6 (14.7)	5.9 (21.2)
<i>I</i> / σ(<i>I</i>) ⁴	15.1 (4.8)	12.6 (3.0)	11.6 (2.6)	6.5 (3.0)	8.6 (3.3)	12.1 (5.5)	11.1 (4.4)	12.2 (4.4)	10.2 (3.3)
Refinement statistics ⁵									
Number of molecules									
Non-hydrogen atoms				23,398					
Water				1,284					
Sulfate				30					
Glycerol				10					
Resolution range (Å)				1.9–25.0					
Number of reflections									
Work set				227,259					
Test set				12,687					
R _{cryst} (%)				14.7					
R _{free} (%)				17.9					
R.m.s. deviations from ideal geometry									
Bonds (Å)				0.014					
Angles (°)				1.4					
Average <i>B</i> -factors (Å ²) ⁶									
Subunit β (monomer 1 and 2)				23.7, 22.6					
Domain α1 ⁷				21.6, 29.5					
Domain α2 ⁷				55.3, 51.3					
Domain α3 ⁷				26.7, 46.8					

¹Except for the native and CO_a data sets (collected at 0.9801 and 0.9340 Å, respectively) statistics were calculated with Friedel mates treated independently.

²MAD data were collected at either side of the Fe absorption edge. Native data were used as the remote wavelength set.

³Data sets at the high energy (low wavelength) side of Zn (1.282 Å), Cu (1.376 Å), Ni (1.482 Å) and Co (1.602 Å) were collected from this CO-treated crystal.

⁴The numbers given within parentheses refer to the highest resolution shell.

⁵For CO_a collected at wavelength 0.9340 Å. This is the highest resolution data set.

⁶After conversion of TLS parameters and their inclusion in individual *B*-factors by *tlsan*⁵⁶.

⁷Values are for the opened and closed forms, respectively.

and either CO or CO₂/reductant, Ni_p²⁺ will be reduced by two electrons, forming Ni_p⁰ and the A_{red2} state (Ni_d²⁺-Ni_p⁰ [Fe₄-S₄]^{2+/1+}). The redox potential of the Ni_p⁰/Ni_p²⁺ pair should be ~-530 mV *versus* Normal Hydrogen Electrode (NHE), the value reported for the D site¹⁰. The redox state of the [Fe₄-S₄] cube appears irrelevant in the ability of the enzyme to accept a methyl group¹⁵, and we have indicated this by designating its core oxidation as '2+ or 1+' in the A_{red2} state.

The Ni_p⁰ proposal is reasonable only if μ²-bridging 'metallo-cysteinate' ligands to Ni_p show bonding properties that mimic neutral ligands with π-accepting capabilities (for example, trialkylphosphines or CO). Darenbourg *et al.*²⁵ have found that the negative charge of thiolates is effectively neutralized by bridging to two metal centers (so called 'metalated' thiolates). The effect of such ligands on CO stretching frequencies of Fe carbonyl complexes is similar to that of phosphines²⁶. Metalation

increases Ni^{2+/1+} E⁰ values, rendering such compounds more easily reduced. Along the same lines, Reedijk *et al.*²⁷ synthesized a dinuclear Fe-S complex containing a thiolate ligand μ²-bridged to Ni⁰(CO)₃. Stretching CO frequencies in this complex are similar to those of (*t*-butyl)₃P-Ni⁰(CO)₃ (ref. 28), indicating similar electronic properties for the phosphine and metallothiolate. Accordingly, the mechanistic roles of Ni_d²⁺ and the [Fe₄-S₄]²⁺ cube could be restricted to metalate the cysteine ligands of Ni_p to facilitate reduction to the Ni_p⁰ state.

If validated by experimental and theoretical studies, our proposal for Ni_p⁰ would be appealing because there is a rich history of Ni⁰ organometallic phosphine complexes that are catalysts for related reactions, such as the copolymerization of CO with ethylene^{29,30}. Hsiao *et al.*³¹ have shown that CH₃I reacts with mononuclear Ni⁰P₂S₂ (P = phosphine and S = thioether) complexes to yield Ni²⁺-CH₃ adducts into which CO inserts rapidly to form



Ni²⁺-acetyl. The parent Ni²⁺ compounds can be reduced to the Ni¹⁺ state that binds CO. Corresponding Ni²⁺(N₂S₂) (S = thiolate) complexes neither reduce to Ni¹⁺ or Ni⁰ states nor bind CO. Taken together, the reactivity of these compounds supports the possible role of Ni_p⁰ in catalysis and suggests, as indicated above, that Ni_d does not participate directly in acetyl synthesis.

The occurrence of Ni⁰ in the active site of this enzyme would be unprecedented in biology. Thus, subsequent studies are required to assess the feasibility of this hypothesis. The Ni⁰ assignment is formal, as the electron density will be significantly delocalized over the π -accepting ligands³². The important point is that Ni_p and its ligands can donate two electrons to form the CH₃-Ni²⁺ species. A formal Ni⁰ assignment has also been proposed for the reduced Ni-R form of NiFe hydrogenases; in this case, the Ni ion is thought to be protonated and, consequently, isoelectronic with Ni²⁺-H⁻ (ref. 33).

Acetyl-CoA synthesis by ACS/CODH_{mt}

As stated above, one important point is that the enzyme is active for catalysis when Ni_p is in the Ni⁰ redox state and thus capable of binding CO and CH₃-Co³⁺FeSP. This state is derived from reduction of a species containing Ni²⁺ at the proximal site, as suggested by the results of phen treatment¹⁴. Ni_p⁰ with or without bound CO would be a powerful nucleophile that would attack the methyl group of CH₃-Co³⁺FeSP directly, forming Co¹⁺FeSP and either Ni_p²⁺-CH₃ or *cis* C(O)-Ni_p²⁺-CH₃. With both CO and methyl bound to Ni_p²⁺, insertion of the former or migration of the latter would form the acetyl intermediate Ni_p²⁺-C(O)CH₃. Finally, CoA-SH would bind, deprotonate, and attack this intermediate, yielding acetyl-CoA and the Ni_p⁰ state by reductive elimination (Fig. 5a).

A second important point is the presence of two α subunit conformations. This raises the possibility that conformational changes that occur during catalysis dictate the sequence in which substrates and products enter, react and leave the active site. Also, α_o appears to have a CoA-binding pocket that is much less obvious in α_c (data not shown). Because the tunnel entrance at the A_c-cluster is open while the counterpart at the A_o-cluster site is blocked, delivery of CO may be causally connected to the conformation of the α subunit. The protein coordination of the proximal metal site also differs in α_c and α_o subunits, with trigonal pyramidal coordination in α_c and mostly distorted trigonal planar in α_o , suggesting that the geometry of the proximal site is causally related to the conformation of the α subunit. From the structure, the suggestion follows that CO binds to a trigonal pyramidal Ni_p⁰ in the α_c conformation and that CH₃-Co³⁺FeSP binds subsequently. The process of methyl group transfer converts α_c to α_o , and the Ni_p conformation becomes square-pyramidal (with CO bound axially and methyl bound in the plane). Subsequent insertion and CoA attack yield acetyl-CoA, Ni_p⁰ and the α_c conformation (Fig. 5a). One should bear in mind, however, that it is possible to methylate the A-cluster in the absence of CO and then generate acetyl-CoA after subsequent incubation in CO and CoA¹⁰; therefore, the actual sequence of events cannot be deduced from the structure alone.

Comparison to a Cu-based mechanism.

In the crystal structure reported by Doukov *et al.*⁸ the α subunits from each heterotetramer are identical, related by a noncrystallographic two-fold symmetry axis and, as far as we can tell, equivalent to our closed conformation. Their A-clusters contain the same Ni_d site and [Fe₄-S₄] cluster as we observe, but a Cu¹⁺ ion replaces the Zn_p²⁺ of our A_c-cluster and, most important, the

Ni_p of our A_o-cluster. During the first step of acetyl-CoA synthesis, the authors propose that CO binds Cu¹⁺ as it emerges from the hydrophobic tunnel. In their α conformation⁸, as in our α_c , the proximal (Cu) and Ni_d ions are buried below the molecular surface, requiring a significant conformational change to get these metal ions more exposed to the protein surface to accept a methyl group from CH₃-Co³⁺FeSP and subsequently donate an acetyl group to CoA. Although not mentioned explicitly, the cubane appears to have been assigned, at least partially, as the required reducing functionality, so that the methyl group transfers to Ni_d²⁺ in concert with oxidation of the all-ferrous cube (although Ni_d redox could also be implicitly involved). Methyl migration from CH₃-Ni_d²⁺ to Cu¹⁺-CO follows this step, yielding a Cu-acetyl intermediate. Finally, CoA binds, deprotonates and attacks the acetyl group, yielding acetyl-CoA.

The presence of Cu (and possibly Zn)⁸ in the A-clusters and the presence of Zn and Ni in the A-clusters reported here indicate that the proximal site of the A-cluster can bind, and possibly exchange, at least three different metal ions. We believe, however, that once either Cu or Zn binds to the proximal site, the α subunit stays in an inactive conformation because, out of the three ions, only Ni⁰ would be able to undergo the postulated two-electron redox process required for methylation. Although their chemical properties are certainly different, Zn²⁺, Cu¹⁺ and Ni⁰ are all *d*¹⁰ metal ions with identically occupied *d* orbitals and geometry preferences. It is difficult at this point to assert whether metal substitutions occurred within the cell or during or after purification of ACS/CODH.

We are skeptical about the proposed role for Cu in the catalytic mechanism⁸. The reported correlation between Cu content and catalytic activity is not present, as may be shown by normalization of the metal contents reported in Table 2 of Doukov *et al.*⁸. As discussed above, the electron spin of the A-cluster in the state that yields the Ni-Fe-C signal is substantially delocalized among the Ni, the [Fe₄-S₄] cube and CO^{17,34}. With CO bound to Cu (*I* = 3/2) as proposed, it seems unusual that a {Ni¹⁺...Cu¹⁺-CO-[Fe₄-S₄]²⁺} spin-coupled cluster would show strong hyperfine splitting at the Ni, Fe and CO portions but not at the Cu located at the center of the system. The Cu-based structure neither explains the heterogeneity that characterizes this enzyme in terms of nonlabile and labile Ni because only a single type of Ni is observed. Another point concerns the migratory insertion reaction. In model compounds, alkyl-to-acyl insertions typically involves a single metal center with CO and methyl groups bound *cis* to each other³⁵ and not two different metal centers (CO bound to Cu and methyl bound to Ni), as proposed.

Additional evidence for a Ni-Ni-[Fe₄-S₄] active site

During the preparation of this paper, an additional mechanism has been proposed by Gencic and Grahame³⁶ based on metal reconstitution experiments using a recombinant apo ACS subunit from the methanogen *Methanosarcine thermophila*. The Gencic-Grahame mechanism is similar to our own in three respects: (i) it considers only the Ni-Ni-Fe-containing A-clusters as catalytically active, ruling out any Cu-based catalysis, (ii) it does not assign any catalytic properties to Ni_d and (iii) it does not assign a catalytic role to the one-electron reduced species giving rise to the Ni-Fe-C EPR signal because methylation is a two electron process. Instead of proposing a Ni⁰/Ni²⁺ pair as the two-electron donor required to form the methyl-metal bond, Gencic and Grahame postulate a Ni¹⁺/Ni³⁺ pair. In subsequent steps, their mechanism requires one-electron redox chemistry by the [Fe₄-S₄] cluster. This is a major drawback of this model

because, as mentioned above, data from one of our laboratories rules out a catalytically relevant redox active $[\text{Fe}_4\text{-S}_4]$ center at the A-cluster¹⁵. The authors also claim that no external reductant is required to generate the Ni-Fe-C species. However, in this scheme³⁶, the unpaired electron originates from the $[\text{Fe}_4\text{-S}_4]$ cluster, implying that the starting material was already at least partially reduced by an external reductant.

In light of the binuclear Ni-based A_0 structure reported here, the known requirement of ACS for two Ni equivalents to support catalytic activity, the inorganic chemistry and spectroscopy favoring Ni, the promiscuity and lability of the proximal site and the varying levels of Cu observed in active enzyme solutions, we do not favor a Cu-based mechanism for ACS catalysis. Instead, we believe that active A-clusters are composed of a $[\text{Fe}_4\text{-S}_4]\text{-Ni}_p\text{-Ni}_d$ unit where only Ni_p is active, possibly as a $\text{Ni}^0/\text{Ni}^{2+}$ redox pair.

Methods

Purification and crystallization. *M. thermoacetica* cells were grown as described³⁷. ACS/CODH_{Mt} was purified as reported^{14,17} with only minor modifications. A monoclinic, space group C2 crystal form with $a = 245 \text{ \AA}$, $b = 82 \text{ \AA}$, $c = 167 \text{ \AA}$, $\beta = 96^\circ$ and one $\alpha_2\beta_2$ dimer per asymmetric unit was obtained in 2–4 μl hanging drops in an anaerobic glove box at 20 °C. Hanging drops were prepared by mixing an equal volume of a ACS/CODH_{Mt} solution at 10 mg ml⁻¹ in 50 mM Tris-HCl, pH 8.0, 2 mM sodium dithionite and 10 mM dithiothreitol with the crystallization solution. The latter contained 1.95–2.10 M ammonium sulfate, 100 mM HEPES buffer, pH 7.0–7.3, 3–5% (w/v) PEG 400, 2 mM sodium dithionite and 100–200 mM dimethylethyl ammonium propane sulfonate (the NDSB195 reagent). Crystals were detected about one year after setting the crystallization plates. CO- and Xe gas-binding experiments and anaerobic flash-cooling of ACS/CODH_{Mt} crystals were carried out inside the glove box as described³⁸.

Data collection. All the diffraction data were collected at the European Synchrotron Radiation Facility (ESRF), Grenoble, France (Table 2). A 2.2 Å resolution native data set and Fe-edge MAD data were collected at the BM-30A beamline. To identify the nature of the other transition metals present in the protein, four data sets were collected using a CO-treated crystal at the high-energy side of the K-edges of Zn, Cu, Ni and Co at the ID29 beamline of the ESRF. All data were processed with the July 2002 version of XDS³⁹.

Structure determination and refinement. The structure was solved by combining MR and MAD phases. MR was performed with AMoRe⁴⁰ using the known CODH_{Ch} structure (PDB entry 1JJY). A contrasted solution was found for the two β subunits of the dimer using reflections in the 15–3 Å resolution range (correlation coefficient

of 0.35 and R -factor of 0.48.) The positions of seven metal clusters were found both in a native anomalous difference map calculated with MR phases and from Patterson maps calculated with MAD data set using SOLVE⁴¹. These sites were subsequently treated as low-resolution super-atoms for refinement and phase calculations. Phases were combined with SIGMAA⁴² and subsequently significantly improved and extended to 2.2 Å resolution by density modification, including two-fold electron density averaging, using RESOLVE⁴³.

After applying the correct amino acid sequence to the ACS/CODH_{Mt} β subunit placed using MR, the protein model for the α subunit was progressively built with the initial help of automatic tracing using warpNtrace⁴⁴ and RESOLVE⁴³ and the graphics program TURBO-FRODO⁴⁵. Initial density-averaged maps showed well-defined electron density at the N-terminal domain of the α subunit but ill-defined density elsewhere. This was subsequently explained by the different orientations of the central and C-terminal domains in the two α subunits, which did not allow for automatic noncrystallographic two-fold symmetry electron density averaging to be effectively applied. Phases from the partially refined model containing the β_2 dimer and the α N-terminal domains of ACS/CODH_{Mt}, combined with the experimental MAD phases, produced increasingly well-defined electron density maps. Several cycles of model building and model and MAD phase combination resulted in the complete structure. The same unique set of reflections (5% of the total) was excluded for the refinement of all crystal structures. Crystallographic refinement was performed with REFMAC5 (ref. 46) using eight TLS groups⁴⁷, one for each of the three domains of each α subunit and one for each β monomer. When the CO_s data set became available, the model was further refined to a resolution of 1.9 Å. Refinement statistics are given in Table 2.

Coordinates. Atomic coordinates and structure factors corresponding to the 1.9 Å resolution model of the CO-treated crystal have been deposited with the Protein Data Bank (accession code 1OAO).

Acknowledgments

We thank T. Rabilloud for preparing the NDSB195 reagent and M.Y. Darensbourg for helpful discussion about the feasibility of a Ni_p^0 state. This study was supported by the Robert A. Welch Foundation, the National Institutes of Health and by the CEA and the CNRS through institutional funding. We also thank L. Martin for excellent technical help. We appreciate the help with X-ray data collection from the following scientists working at the European Synchrotron Radiation Facility: L. Jacquamet and M. Pirocchi (LCCP and BM30), J. McCarthy (ID14EH1) and G. Sainz (ID29).

Competing interests statement

The authors declare that they have no competing financial interests.

Received 11 December, 2002; accepted 24 February, 2003.

1. Huber, C. & Wachtershauser, G. Activated acetic acid by carbon fixation on (Fe, Ni)S under primordial conditions. *Science* **276**, 245–247 (1997).
2. Wood, H.G. & Ljungdahl, L.G. Autotrophic character of acetogenic bacteria. in *Variation in Autotrophic Life* (eds. Shively, J.M. & Barton, L.L.) 201–250 (Academic Press, New York; 1991).
3. Dobbek, H., Svetlitchnyi, V., Gremer, L., Huber, R. & Meyer, O. Crystal structure of a carbon monoxide dehydrogenase reveals a [Ni-4Fe-5S] cluster. *Science* **293**, 1281–1285 (2001).
4. Drennan, C.L., Heo, J., Sintchak, M.D., Schreiber, E. & Ludden, P.W. Life on carbon monoxide: X-ray structure of *Rhodospirillum rubrum* Ni-Fe-S carbon monoxide dehydrogenase. *Proc. Natl. Acad. Sci. USA* **98**, 11973–11978 (2001).
5. Lindahl, P.A., Munck, E. & Ragsdale, S.W. CO dehydrogenase from *Clostridium thermoaceticum*. EPR and electrochemical studies in CO₂ and argon atmospheres. *J. Biol. Chem.* **265**, 3873–3879 (1990).
6. Maynard, E.L. & Lindahl, P.A. Evidence of a molecular tunnel connecting the active sites for CO₂ reduction and acetyl-CoA synthesis in acetyl-CoA synthase from *Clostridium thermoaceticum*. *J. Am. Chem. Soc.* **121**, 9221–9222 (1999).
7. Seravalli, J. & Ragsdale, S.W. Channeling of carbon monoxide during anaerobic carbon dioxide fixation. *Biochemistry* **39**, 1274–1277 (2000).
8. Doukov, T.I., Iverson, T.M., Seravalli, J., Ragsdale, S.W. & Drennan, C.L. A Ni-Fe-Cu center in a bifunctional carbon monoxide dehydrogenase/acetyl-CoA synthase. *Science* **298**, 567–572 (2002).
9. Lu, W.P., Harder, S.R. & Ragsdale, S.W. Controlled potential enzymology of methyl transfer reactions involved in acetyl-CoA synthesis by CO dehydrogenase and the corrinoid/iron-sulfur protein from *Clostridium thermoaceticum*. *J. Biol. Chem.* **265**, 3124–3133 (1990).
10. Barondeau, D.P. & Lindahl, P.A. Methylation of carbon monoxide dehydrogenase from *Clostridium thermoaceticum* and the mechanism of acetyl-CoA synthesis. *J. Am. Chem. Soc.* **119**, 3959–3970 (1997).
11. Ragsdale, S.W. & Wood, H.G. Acetate biosynthesis by acetogenic bacteria. Evidence that carbon monoxide dehydrogenase is the condensing enzyme that catalyzes the final steps of the synthesis. *J. Biol. Chem.* **260**, 3970–3977 (1985).
12. Tucci, G.C. & Holm, R.H. Nickel-mediated formation of thio esters from bound methyl, thiols, and carbon monoxide: a possible reaction pathway of acetyl-coenzyme A synthase activity in nickel-containing carbon monoxide dehydrogenases. *J. Am. Chem. Soc.* **117**, 6489–6496 (1995).
13. Montet, Y. et al. Gas access to the active site of Ni-Fe hydrogenases probed by X-ray crystallography and molecular dynamics. *Nat. Struct. Biol.* **4**, 523–526 (1997).
14. Shin, W. & Lindahl, P.A. Function and CO binding properties of the NiFe complex in carbon monoxide dehydrogenase from *Clostridium thermoaceticum*. *Biochemistry* **31**, 12870–12875 (1992).
15. Tan, X.S., Sewell, C., Yang, Q. & Lindahl, P.A. Reduction and methyl transfer kinetics of the α subunit from acetyl-coenzyme A synthase. *J. Am. Chem. Soc.* **125**, 318–319 (2003).
16. Tan, X.S., Sewell, C. & Lindahl, P.A. Stopped-flow kinetics of methyl group transfer between the corrinoid-iron-sulfur protein and acetyl-coenzyme A synthase from *Clostridium thermoaceticum*. *J. Am. Chem. Soc.* **124**, 6277–6284 (2002).
17. Ragsdale, S.W., Ljungdahl, L.G. & Dervartanian, D.V. ¹³C and ⁶¹Ni isotope substitutions confirm the presence of a nickel(III)-carbon species in acetogenic CO dehydrogenases. *Biochem. Biophys. Res. Commun.* **115**, 658–665 (1983).
18. Ragsdale, S.W., Wood, H.G. & Antholine, W.E. Evidence that an iron-nickel-carbon complex is formed by reaction of carbon monoxide with the carbon monoxide dehydrogenase from *Clostridium thermoaceticum*. *Proc. Natl. Acad. Sci. USA* **82**, 6811–6814 (1985).
19. Xia, J. & Lindahl, P.A. Assembly of an exchange-coupled [Ni:Fe₄S₄] cluster in the α metallosubunit of CO dehydrogenase from *Clostridium thermoaceticum* with spectroscopic properties and CO-binding ability mimicking those of the acetyl-CoA synthase active site. *J. Am. Chem. Soc.* **118**, 483–484 (1996).
20. Russell, W.K., Stålhandske, C.M.V., Xia, J., Scott, R.A. & Lindahl, P.A. Spectroscopic, redox and structural characterization of the Ni-labile and nonlabile forms of the acetyl-CoA synthase active site of CO dehydrogenase. *J. Am. Chem. Soc.* **120**, 7502–7510 (1998).
21. Shin, W., Anderson, M.E. & Lindahl, P.A. Heterogeneous nickel environments in carbon monoxide dehydrogenase from *Clostridium thermoaceticum*. *J. Am. Chem. Soc.* **115**, 5522–5526 (1993).
22. Shin, W. & Lindahl, P.A. Low spin quantitation of NiFeC EPR signal from carbon monoxide dehydrogenase is not due to damage incurred during protein purification. *Biochim. Biophys. Acta* **1161**, 317–322 (1993).
23. Lindahl, P.A., Ragsdale, S.W. & Münck, E. Mössbauer study of CO dehydrogenase from *Clostridium thermoaceticum*. *J. Biol. Chem.* **265**, 3880–3888 (1990).
24. Wilson, B.E. & Lindahl, P.A. Equilibrium dialysis study and mechanistic implications of coenzyme A binding to acetyl-CoA synthase/carbon monoxide dehydrogenase from *Clostridium thermoaceticum*. *J. Biol. Inorg. Chem.* **4**, 742–748 (1999).
25. Musie, G., Farmer, P.J., Tuntulani, T., Reibenspies, J.H. & Darensbourg, M.Y. Influence of sulfur metalation on the accessibility of the Ni^{III} couple in [N, N'-Bis(2-mercaptoethyl)-1,5-diazacyclooctano]nickel(II): insight into the redox properties of [NiFe]-hydrogenase. *Inorg. Chem.* **35**, 2176–2183 (1996).
26. Lai, C.-H., Reibenspies, J.H. & Darensbourg, M.Y. Thiolate bridged nickel-iron complexes containing both iron(0) and iron(II) carbonyls. *Angew. Chem. Int. Ed. Engl.* **35**, 2390–2393 (1996).
27. Bouwman, E., Henderson, R.K., Spek, A.L. & Reedijk, J. Spontaneous assembly of a novel tetranuclear Ni-Fe complex by complete reshuffling of ligands and oxidation states. *Eur. J. Inorg. Chem.* **1999**, 217–219 (1999).
28. Tolman, C.A. Electron donor-acceptor properties of phosphorus ligands. Substituent additivity. *J. Am. Chem. Soc.* **92**, 2953–2956 (1970).
29. Shultz, C.S., DeSimone, J.M. & Brookhart, M. Four- and five-coordinate CO insertion mechanisms in d⁸-nickel(II) complexes. *J. Am. Chem. Soc.* **123**, 9172–9173 (2001).
30. Tolman, C.A., Seidel, W.C. & Gosser, L.W. Formation of three-coordinate nickel(0) complexes by phosphorus ligand dissociation from NiL₄. *J. Am. Chem. Soc.* **96**, 53–60 (1973).
31. Hsiao, Y.-M., Chojnacki, S.S., Hinton, P., Reibenspies, J.H. & Darensbourg, M.Y. Organometallic chemistry of sulfur/phosphorus donor ligand complexes of nickel(II) and nickel(0). *Organometallics* **12**, 870–875 (1993).
32. Cotton, F.A. & Wilkinson, G. The chemistry of the transition elements. in *Advanced Inorganic Chemistry* 5th edn. 741–754 (Wiley, New York; 1997).
33. Volbeda, A. et al. Structure of the (NiFe) hydrogenase active site: evidence for biologically uncommon Fe ligands. *J. Am. Chem. Soc.* **118**, 12989–12996 (1996).
34. Fan, C., Gorst, C.M., Ragsdale, S.W. & Hoffman, B.M. Characterization of the nickel-iron-carbon complex formed by reaction of carbon monoxide with the carbon monoxide dehydrogenase from *Clostridium thermoaceticum* by Q-band ENDOR. *Biochemistry* **30**, 431–435 (1991).
35. Collman, J.P., Hegedus, L.S., Norton, J.R. & Finke, R.G. Intramolecular insertion reactions. in *Principles and Applications of Organotransition Metal Chemistry* 355–399 (University Science Books, Mill Valley; 1987).
36. Gencic, S. & Grahame, D.A. Nickel in subunit β of the acetyl-CoA decarbonylase/synthetase multienzyme complex in methanogens. *J. Biol. Chem.* **278**, 6101–6110 (2003).
37. Lundie, L.L. Jr. & Drake, H.L. Development of a minimally defined medium for the acetogen *Clostridium thermoaceticum*. *J. Bacteriol.* **159**, 700–703 (1984).
38. Vernède, X. & Fontecilla-Camps, J.C. A method to stabilize reduced and/or gas-treated protein crystals by flash-cooling under a controlled atmosphere. *J. Appl. Crystallogr.* **32**, 505–509 (1999).
39. Kabsch, W. Integration, scaling, space-group assignment and post refinement. in *International Tables for Crystallography, Volume F, Crystallography of Biological Macromolecules* (eds. Rossmann, M.G. & Arnold, E.) Ch. 11.3 (Kluwer Academic Publishers, Dordrecht; 2001).
40. Navaza, J. AMoRe: an automated package for molecular replacement. *Acta Crystallogr. A* **50**, 157–163 (1994).
41. Terwilliger, T.C. & Berendzen, J. Automated structure solution for MIR and MAD. *Acta Crystallogr. D* **55**, 849–861 (1999).
42. Read, R.J. Improved Fourier coefficients for maps using phases from partial structures with errors. *Acta Crystallogr. A* **42**, 140–149 (1986).
43. Terwilliger, T.C. Map-likelihood phasing. *Acta Crystallogr. D* **57**, 1763–1775 (2001).
44. Perrakis, A., Morris, R.J. & Lamzin, V.S. Automated protein model building combined with iterative structure refinement. *Nat. Struct. Biol.* **6**, 458–463 (1999).
45. Roussel, A. & Cambillau, C. *Turbo-Frodo* (Silicon Graphics, Mountain View; 1989).
46. Murshudov, G.N., Vagin, A.A. & Dodson, E.J. Refinement of macromolecular structures by the maximum-likelihood method. *Acta Crystallogr. D* **53**, 240–255 (1997).
47. Winn, M.D., Isupov, M.N. & Murshudov, G.N. Use of TLS parameters to model anisotropic displacements in macromolecular refinement. *Acta Crystallogr. D* **57**, 122–133 (2001).
48. Volbeda, A. Spéologie des hydrogenases à nickel et à fer. *Les écoles physique et chimie du vivant* **1**, 47–52 (1999).
49. Collaborative Computational Project, Number 4. The CCP4 suite: programs for protein crystallography. *Acta Crystallogr. D* **50**, 760–763 (1994).
50. Kraulis, P.J. MOLSCRIPT: a program to produce both detailed and schematic plots of protein structures. *J. Appl. Crystallogr.* **24**, 946–950 (1991).
51. Merritt, E.A. & Bacon, D.J. Raster3D: photorealistic molecular graphics. *Methods Enzymol.* **277**, 505–524 (1997).
52. Lawrence, M.C. & Bourke, P. A program for generating electron density isosurfaces from Fourier syntheses in protein crystallography. *J. Appl. Crystallogr.* **33**, 990–991 (2000).